Appl. Phys. B 69, 459–465 (1999) / Digital Object Identifier (DOI) 10.1007/s003409900115

Applied Physics B
Lasers
and Optics

Portable fiber-coupled diode-laser-based sensor for multiple trace gas detection

D.G. Lancaster, D. Richter, F.K. Tittel

Rice Quantum Institute, Rice University, Houston, TX 77251-1892, USA
Fax: +1-713/524-5237, Email: davelanc@rice.edu

Received: 14 May/Revised version: 24 June 1999/Published online: 30 September 1999

Abstract. Tunable narrowband mid-infrared radiation from 3.25 to 4.4 μm is generated by a compact fiber-coupled, difference-frequency-based spectrosopic source. A 20-mW external cavity diode laser (with a tuning range from 814 to 870 nm) and a 50-mW distributed-Bragg-reflector diode-laser-seeded ytterbium-doped fiber amplifier operating at 1083 nm are difference-frequency mixed in a multi-grating, temperature-controlled periodically poled $LiNbO_3$ crystal. A conversion efficiency of 0.44 mW/(W^{2}cm) (corresponding to a power of ≈ 3 μW at 3.3 μm) represents the highest conversion efficiency reported for a portable device. Performance characteristics of such a sensor and its application to spectroscopic detection of CO_2, N_2O, H_2CO, HCl, NO_2, and CH_4 will be reported in this work.

PACS: 42.62 Fi; 33.20 Ea; 42.60 By

Difference-frequency mixing of near-infrared cw laser sources is a convenient technique to spectrally shift visible and infrared lasers into the mid-infrared spectral region. By utilizing the recent commercial availability of novel nonlinear optical materials such as periodically poled lithium niobate (PPLN), and frequency-stable single-mode diode lasers in the 0.8 to 1.5 μm spectral region, the key opto-electronic components exist to readily generate microwatt-level radiation in the 3 to 5 μm range [1]. This spectral region is significant as many molecules have strong fundamental rovibrational absorption lines which permit sensitive and absolute concentration measurements. Our motivation is to develop a compact difference-frequency based trace gas sensor that is widely tunable, rugged and cost effective. The requirements for such a sensor include room temperature and real-time operation, narrow bandwidth to minimize spectral interference, adequate signal-to-noise for the available infrared detectors, a robust design (suitcase size), inherent frequency stability (with no mode-hopping behavior), and wide wavelength tunability for multiple trace gas species detection.

In recent work, this group has reported trace gas sensors generating microwatt-level radiation based on difference-frequency mixing (DFM) (using discrete optical components positioned on a compact optical bench) of Fabry–Pérot style diode lasers with a Nd:YAG laser [2] and a 1083-nm distributed Bragg reflector (DBR) diode laser [3]. The former system proved robust enough to be used in a successful one-month field test involving high-sensitivity H_2CO detection [4]. Widely tunable and hence multi-component capable systems based on DFM of an extended cavity diode laser (ECDL) and Nd:YAG laser have been reported in [5] and [6], but these systems are typically sub microwatt and also alignment-critical. We have also reported laboratory prototype sensors that difference-frequency mix (in PPLN) frequency-stable diode lasers and utilize single-mode fiber delivery and rare-earth-doped fiber amplifiers producing up to 11 μW of radiation [7, 8]. The use of fiber delivery and fiber beam combining in these systems eliminates most of the routine alignment and stability problems associated with a difference-frequency mixed source. In this work we report an optical sensor architecture that is widely tunable (with virtually no re-alignment required) and packaged for portable field operation.

The sensor difference-frequency mixes two frequency-stable pump diode lasers, namely an ECDL employing a high-power single-frequency InGaAs laser and a 1083-nm distributed-Bragg-reflector (DBR) diode laser. Moreover, we have taken advantage of recent developments in fiber amplifier technology [9] to increase the pump power delivered to the nonlinear optical crystal.

Details of the development of a field-ready fiber-based DFG sensor and significantly improved conversion efficiency as compared to previous DFG architectures are reported. In fact several important trace gases can be accessed in the operating range of this DFG sensor from 3.25 to 4.4 μm. We have investigated the difference-frequency mixing conversion efficiency as a function of mid-infrared wavelength and compared it to the theoretically expected efficiency. The predicted and experimentally measured PPLN phasematching conditions were also determined. Wide wavelength tunability was demonstrated and spectroscopic scans of six trace gases are reported.

1 Experimental configuration

The sensor, as shown in Fig. 1, consists of a 25-mW ECDL which is continuously tunable from 814 to 870 nm (no mode-hopping behavior is observed), and a 50-mW 1083-nm distributed-Bragg-reflector diode laser (DBR). The output from the DBR diode laser is collimated using an aspheric lens, passes through a −45 dB optical-isolator, and is then coupled into standard 6.6-μm-core diameter single-mode optical fiber terminated with a FC-APC style connector (threaded connector with the tip polished at 8° from normal incidence). A power of 12 mW of the seed radiation from the DBR diode laser is launched into the fiber. To increase the mechanical rigidity of the coupling arrangement, no beam correction optics were used and the entire diode/optics assembly was mounted on a compact stainless steel miniature-bench. Although higher coupling efficiencies into the fiber can be achieved, this was not necessary for this application, as only several mW of injected power at 1083 nm was required to saturate the Yb fiber amplifier. An amplifier output power of 590 mW at 1083 nm is obtained. The fiber was fusion-spliced to the counter-propagating side (with respect to the 975-nm pump) of a 7.2-m ytterbium doped fiber amplifier pumped by a 975-nm, 2-W-diode laser. A V-groove geometry was used to launch the amplifier pump light into the Yb^{3+} doped double-cladding fiber [9, 10]. All amplifier components were packaged into a $9 \times 11 \times 2$ cm housing.

The ECDL pump beam is also passed through a −30 dB opto-isolator, and was launched into a 5.5-μm-core-diameter SLM fiber using a single fiber-port assembly with a 48% optical coupling efficiency. Coarse frequency tuning of a Littman-type ECDL was achieved by 'rotation' of its tuning mirror with respect to the diffraction grating. The advantage of the Littman ECDL configuration is the consistent beam-pointing stability as a function of wavelength over the entire ECDL tuning range, ensuring consistent coupling into the optical fiber. Fine tuning and approximately linear repetitive scanning (at < 200 Hz) over single or multi-component absorption lines of up to ≈ 25 GHz (0.83 cm^{-1}) was accomplished by linear current modulation of the DBR diode laser. Tuning the DBR diode laser was used in preference to the slower, non-linear tuning available from the piezoelectrically modulated grating of the ECDL that tended to reduce its spectral stability.

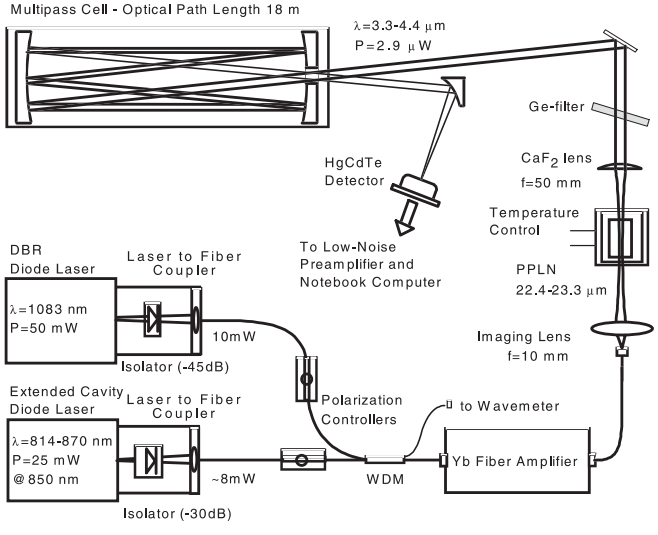

Fig. 1. Schematic diagram of the extended cavity diode laser and diode-laser-seeded 1083-nm Yb amplifier pumped difference-frequency spectrometer

The pump wavelengths were combined by a four-port fiber coupler (2 in, 2 out), with losses of 9% and 8% at 1083 and 830 nm, respectively. An additional advantage of the fiber coupler is the availability of several percent of each wavelength at the second output fiber, thereby allowing the use of an on-line fiber-coupled wavemeter for frequency monitoring of the pump light. The linear polarization output from the launch fiber for a $e + e \rightarrow e$ difference-frequency generation (DFG) process in the PPLN crystal was maintained by using two polarization controllers (in-line: PolaRITE) in the fiber delivery system. An achromat lens ($f = 10$ mm; 0.25 NA) was used for imaging the fiber output (terminated with a FC-APC connector) into the PPLN crystal. A 19-mm-long, 0.5-mm-thick PPLN crystal with a broadband AR-coating applied to both end faces contained 8 quasi-phasematching channels (0.5 mm wide) from 22.4–23.1 μm in 0.1-μm increments. The PPLN crystal was mounted on a temperature-controlled copper block ($20 \times 15 \times 10$ mm) heated by a resistive element that allowed the crystal to be operated at higher temperatures (< 250 °C). The temperature at the copper block surface was measured by a cold-junction compensated thermocouple (2% accuracy). To reduce the thermal resistance between the copper block and crystal, thermal heat-sink compound was used. In the portable sensor configuration, the PPLN crystal was mounted on a Peltier element and the temperature monitored by a 10-KΩ thermistor. This allowed operation at regulated temperatures from 10 to 85 °C. The lower temperature limit was set by concern for water condensation on the crystal faces.

The DFG radiation was collimated by a 5-cm-focal-length CaF_2 lens and the residual pump light was blocked by a 3-mm-thick AR-coated germanium filter. The radiation was either focused directly on the three-stage Peltier-cooled HgCdTe (MCT) detector for power measurements or aligned through a 18-m-pathlength multi-pass spectroscopic cell (physically 30 cm long) and then focused onto the detector. In both cases the radiation was focused onto the detector by use of a 5-cm-focal-length gold-coated off-axis parabolic mirror. The MCT detector, with a 1-mm^2 active area and a measured noise equivalent power of 3 $pW/Hz^{-1/2}$, was dc-coupled to a low-noise pre-amplifier operating in a photoconductive mode.

In order to reduce the size of the driver electronics required for the DBR diode laser, Yb amplifier, and PPLN crystal Peltier element, compact OEM diode laser current and thermoelectric (TE) drivers were used. A TTL-triggered relay controlled a beam shutter placed in front of the ECDL to allow a measurement of the detector dark voltage required for absolute transmission measurements. The data acquisition system used is similar to the one described in [4], and consisted of the output of the MCT detector pre-amplifier interfaced via a PCMCIA 16-bit A-D card to a notebook computer (266 MHz Pentium II running Windows 95). Detector voltage was sampled at a rate of 100 kHz with a 9-kHz low-

pass filter (software-implemented Gaussian filter). The data acquisition and analysis were controlled by the Labview programming language.

The sensor including all electronics was placed on a 45×45 cm optical breadboard, with an overall height of 12 cm. The weight was 25 kg and the entire sensor was then mounted in a reinforced plastic suitcase for portability. Power was supplied by 4×5 V, 2-A linear power supplies, and $2 \times \pm 15$ V, 200-mA linear power supplies. The ECDL used its commercial power supply and driver. Total power consumption is estimated at 60 W.

To provide a continuous gas flow through the spectroscopic cell, at a regulated pressure, a two-stage diaphragm pump was used in series with a pressure flow controller. A miniature Baratron pressure transducer (MKS-722) was used to measure the gas pressure just prior to the multi-pass cell. To reduce the interaction between the gas handling components and the gas mixtures, stainless steel tubing was used throughout the gas delivery system. Furthermore, for measurement of reactive gases (such as H_2CO, HCl and NO_2) the gas handling system was maintained at $\approx 40\,^{\circ}$C by use of heating tape. For the measurement of HCl, which reacts strongly with water, and is in addition strongly polar, the gas system was purged for several hours by the use of high-purity N_2 (H_2O concentration specified to be < 5 ppm).

2 Experimental results

The mid-infrared power (DFG idler) as a function of wavelength is shown in Fig. 2. The right hand axis is the ECDL power (pump) incident on the crystal. The 1083-nm power (signal) is kept constant at 540 mW. For incident powers of 6.2 mW and 540 mW of the pump and signal beams, respectively, a maximum idler power of 2.8 μW at 3.46 μm was generated (corrected for losses of 3.4% from the CaF_2 lens and a $\approx 4\%$ wavelength-dependent loss of the Ge filter). The ECDL power delivered by the fiber is 8.5 mW near 850 nm, corresponding to the gain center of the ECDL. In Fig. 3 the mid-infrared conversion efficiency as a function of the idler wavelength is shown and overlaid on this figure is also the expected λ^{-2} dependence of the power conversion. The discrepancy between experimental results and the expected wavelength dependence at longer wavelengths is principally the result of absorption losses in the $LiNbO_3$ crystal beyond 4.0 μm ($\alpha \approx 0.3\,\mathrm{cm}^{-1}$ at 4.2 μm [11]), and a strong CO_2 band from 4.1 to 4.4 μm responsible for absorption of the IR radiation between the crystal and IR detector. The peak DFG conversion efficiency measured was $0.88\,\mathrm{mW/W^2}$ for the 19-mm-long crystal at 3.3 μm. In comparison, the theoretical DFG conversion efficiency yields $1.69\,\mathrm{mW/W^2}$ [12]. Factors that contribute to the reduced experimental conversion efficiency include differing pump-beam mode field diameters in the fiber ($1/e^2$ diameters: 850 nm ≈ 5.5 μm, 1083 nm ≈ 6.6 μm) leading to incomplete overlap of the imaged pump beams in the crystal. The low NA (0.25) of the imaging lens will introduce spherical aberration into the focused beam spots. Some non-uniformity in con-

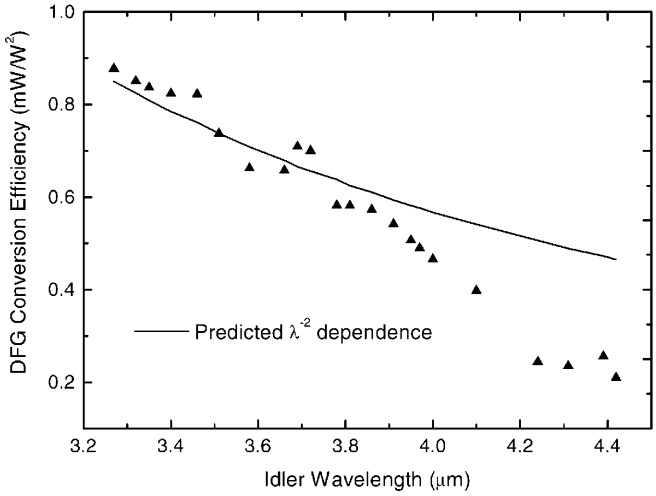

Fig. 3. DFG conversion efficiency as a function of idler wavelength. The expected λ^{-2} wavelength dependence is superimposed. The theoretically predicted conversion efficiency is $1.69\,\mathrm{mW/W^2}$ at 3.3 μm [12]

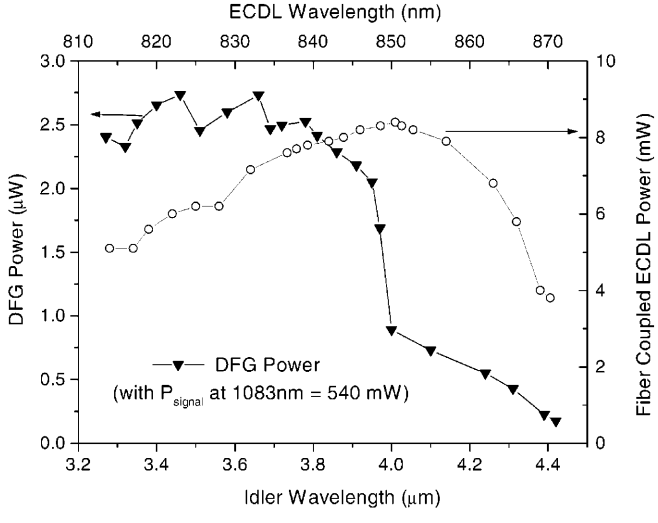

Fig. 2. DFG power as a function of idler wavelength and the ECDL power coupled into the optical fiber as a function of ECDL wavelength

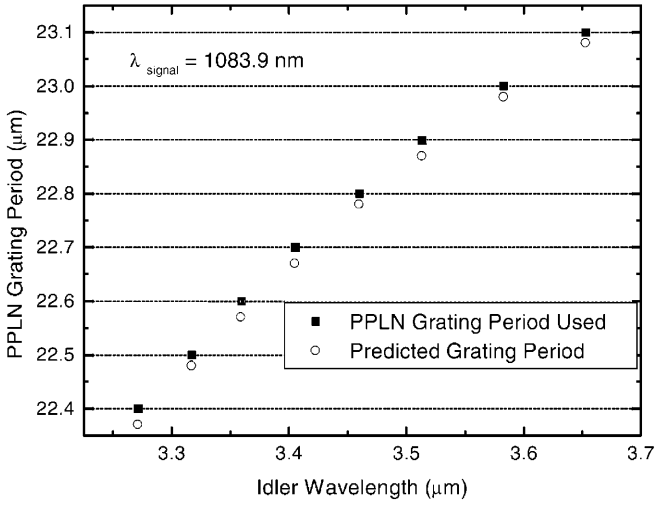

Fig. 4. Measured and theoretically predicted quasi-phasematching (QPM) conditions of the $L = 19$ mm PPLN crystal for QPM periods of 22.4–23.1 μm at 24 °C

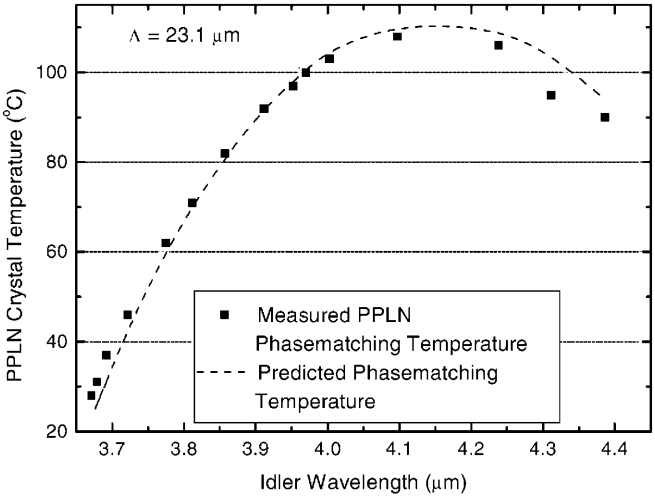

Fig. 5. Measured and theoretically predicted phasematching temperatures as a function of idler wavelength using the 23.1-μm QPM period

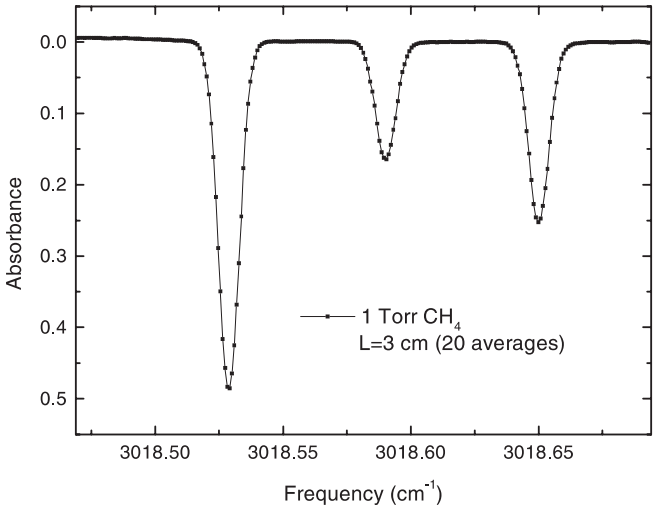

Fig. 6. Q-branch Doppler-broadened 1-Torr CH_4 spectrum near 3.3 μm. By fitting Gaussian absorption peaks to the individual absorption features and de-convolving the peak width with the calculated molecular Doppler width, an estimate of 42 ± 5 MHz was determined for the DFG radiation linewidth (assumed Gaussian)

version efficiency across individual PPLN channels has also been observed.

The measured PPLN phasematching and theoretically predicted phasematching are shown in Figs. 4 and 5 (using the Sellmeier coefficients published by Jundt [13]). For tuning the idler from 3.27–3.65 μm (Fig. 4), the PPLN crystal was translated perpendicular to the optical axis across the 22.4–23.1 μm QPM channels (0.1-μm steps) at a constant temperature of 25 °C. DFG wavelengths of 3.65 to 4.4 μm were phasematched using the 23.1-μm QPM channel and crystal temperatures from 25 to 110 °C (shown in Fig. 5). Agreement between theory and experiments is good (and is within the manufacturer's stated tolerance for the absolute QPM period), verifying that the Sellmeier coefficients for PPLN are accurate out to at least 4.4 μm. This result indicates that any wavelength in the mid-infrared tuning range of this DFG gas sensor can be conveniently accessed using a combination of crystal temperature and grating period.

In a further improvement to the sensor, the PPLN crystal has been replaced with a redesigned crystal (QPM periods of 22.4–23.3 μm in 0.1-μm steps). This allows the entire tuning range of the sensor to be conveniently phasematched using the different grating periods and temperatures from 11 to 43 °C.

The linewidth of the DFG sensor was measured indirectly by acquisition of a low-pressure Doppler-broadened line spectrum. In Fig. 6 a portion of a Q-branch Doppler-broadened (1 Torr) CH_4 spectrum near 3.3 μm in a 3-cm-length cell is shown. This spectrum was acquired at a sweep frequency of 200 Hz, and is an average of 20 scans. By fitting Gaussian absorption peaks to the individual absorption features, and then de-convolving the width with the calculated molecular Doppler width, an estimate of 42 ± 5 MHz ($0.0014\,cm^{-1}$) was determined for the DFG radiation linewidth (assumed to be Gaussian).

Figure 7 shows individual direct absorption spectra of 6 species of interest for trace gas detection that are within the 3.25 to 4.4 μm tuning range of the sensor including (a) CO_2, (b) N_2O, (c) H_2CO, (d) HCl, (e) NO_2, and (f) CH_4. These spectra have been taken at reduced pressure (88 Torr) in a multi-pass cell with an effective path length of 18 m using either calibrated gas mixtures or room air. The Lorentzian line-shape fits to the spectra are shown in Fig. 7, and the integrated line-shape area was then used to calculate the molecular concentrations. The peak-to-peak baseline noise evident from the recorded spectra in Fig. 7 is

Table 1. Data acquisition parameters, measured spectral characteristics and concentrations compared to the spectral data predicted by the HITRAN96 database and the calibrated concentrations of 6 measured trace gas species shown in Fig. 7

Gas species	Scan range / cm^{-1}	Averaging time / s	Pressure / Torr	Scan center / cm^{-1}, (μm)	Linewidth FWHM / cm^{-1}	HITRAN96-Spectra FWHM / cm^{-1}	Measured concentration	Specified concentration	MDC ($L = 18$ m)
CO_2	0.34	2.1	88	2387.2 (4.19)	0.0201	0.0157	444 ppm	Room air	460 ppb
N_2O	0.29	2.1	88	2572.1 (3.89)	0.0223	0.0199	315 ppb	Room air	95 ppb
H_2CO	0.27	2.1	88	2831.7 (3.53)	0.0279	0.0285	860 ppb	862 ± 15 ppb	54 ppb
HCl	0.33	2.1	87	2843.6 (3.52)	0.0239	0.0203	19.5 ppm	24.4 ppm (±5%)	9 ppb
NO_2	0.28	2.1	88	2881.8 (3.47)	0.0180	0.0164 (note: 2 lines)	7634 ppb	13.0 ppm (±5%)	259 ppb
CH_4	0.32	2.1	88	3028.7 (3.30)	0.0191	0.0185	1756 ppb	Room air	23 ppb

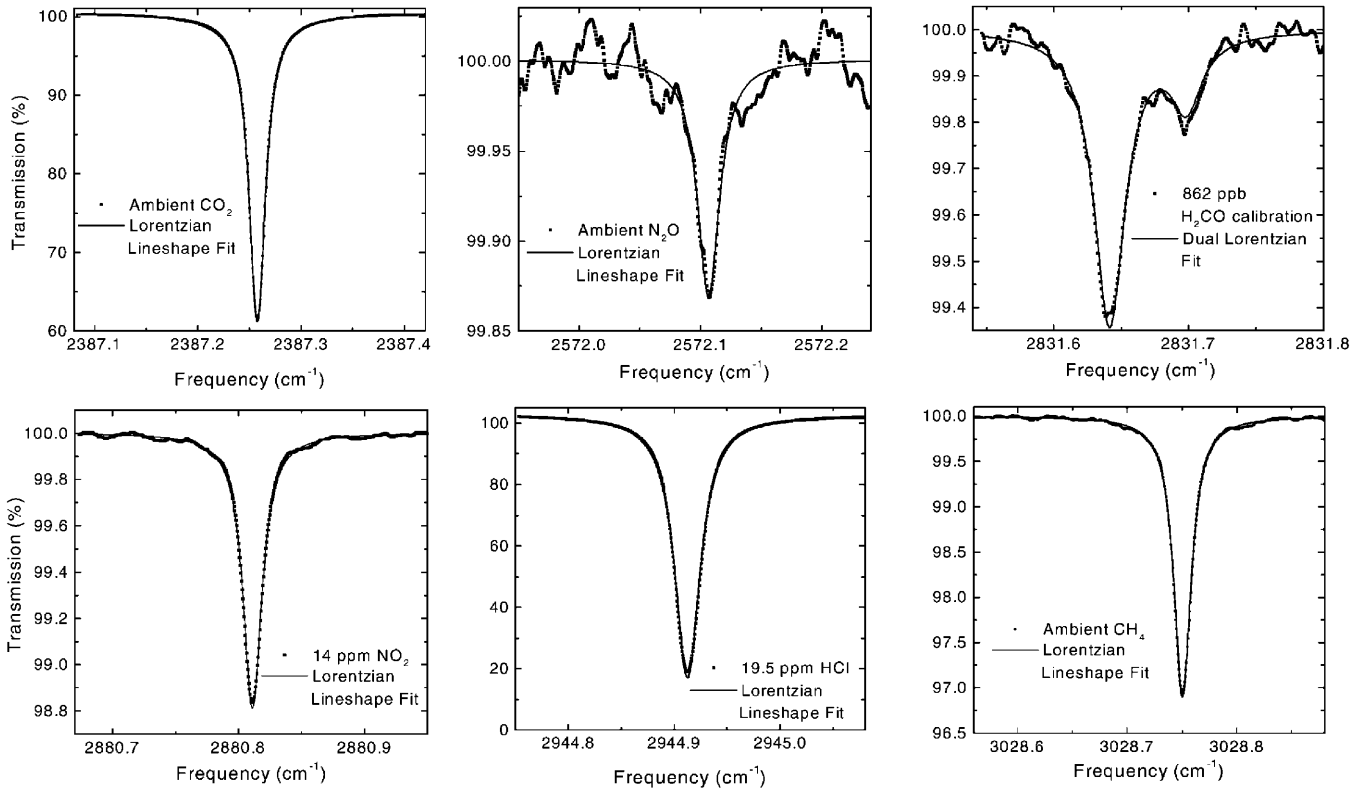

Fig. 7a–f. Individual spectra of **a** CO_2, **b** N_2O, **c** H_2CO, **d** HCl, **e** NO_2, and **f** CH_4. For details see Table 1

±0.02%, and is due to etalon effects in the optical path of the modulated pump beam. To acquire individual spectra, the DFG-based gas sensor was wavelength tuned by manually adjusting the ECDL wavelength (with reference to a wavemeter), and the phasematching conditions of the PPLN crystal were adjusted by a combination of translations to different QPM periods, and temperature changes. No additional re-alignment of the sensor was required when the wavelength was changed indicating that complete automation of the sensor tuning should be straightforward. To remove baseline irregularities caused by etalons in the beam paths, a 3rd-order polynomial was simultaneously fitted with the pressure-broadened Lorentzian line shape using a nonlinear least squares algorithm (Levenberg–Marquardt). For the H_2CO spectrum, which displays two adjacent H_2CO absorption lines, two Lorentzian line shapes were simultaneously fitted with the baseline polynomial function. The data processing and fitting was accomplished in near real-time (< 2 s). For each spectrum the signal was averaged over the specified time, and subsequently the detector dark voltage was measured (50 averages) to allow calculation of the absolute absorption.

In Table 1 the data acquisition parameters are listed, and the measured spectral characteristics and concentrations are compared to the spectral data predicted by the HITRAN96 database and the calibrated concentrations of the measured trace gases. The experimentally measured linewidths of individual species are, in general, broader than the predicted linewidths (from HITRAN96) which is consistent with a measurement of a broadened DFG linewidth. Acquisition of a Doppler-broadened methane spectrum at the time of these spectral measurements revealed a DFG linewidth of 190 MHz. This linewidth was attributed to the 1083-nm diode current driver and after replacing this driver, a narrow DFG linewidth of 42 MHz was subsequently measured (see Fig. 6). In the case of HCl, the concentration was obtained from a calibrated cylinder specified at 24.4 ppm (in N_2) and we measured the HCl concentration to be 19.5 ± 0.2 ppm. This measurement used alternatively the $H^{35}Cl$ line at 2944.913 cm^{-1} and the $H^{37}Cl$

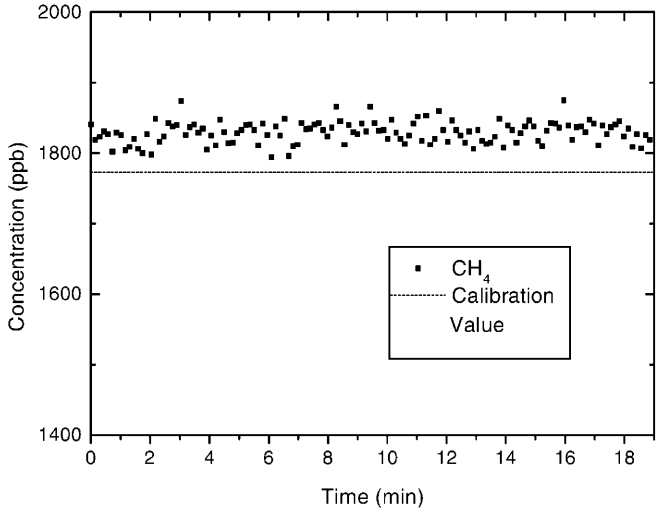

Fig. 8. Measured CH_4 concentration for a 19-min period using a continuously flowing gas mixture at 88 Torr. A spectrum was acquired every 8.7 s and was averaged for 4 s. We measured a concentration of 1829.5 ± 15.4 ppb which compares favorably with the calibrated CH_4 concentration of 1773 ppb [14]

line at 2942.721 cm^{-1} ($S = 5.033 \times 10^{-19}$ cm/molecule and 1.606×10^{-19} cm/molecule, respectively). The minimum detectable concentration (MDC) value stated in Table 1 was calculated for a single measurement, and assumes a $S/N = 1$, and an absorption measurement sensitivity of 4×10^{-4}.

The overall instrument performance, including repeatable precision and suitability of the sensor for long-term measurements was assessed by monitoring of a discrete CH_4 line at 3028.751 cm^{-1} for an extended time period. In this experiment a calibrated 1772.7 ± 1 ppb mixture of CH_4 in air [14] continuously flowed through the multi-pass cell at a pressure of 88 Torr. The experimental results are shown in Fig. 8. Over a 19-min period (131 measurements, 4 s average per measurement), the gas sensor measured a concentration of 1830 ppb, which is within 3.1% of the calibrated concentration (this CH_4 concentration measurement used the HITRAN96 predicted linestrength of 9.519×10^{-20} cm/molecule for the 3028.751 cm^{-1} line). The measurement standard deviation was $\pm 0.8\%$ (± 15 ppb) which corresponds to absorption sensitivities of $\pm 2 \times 10^{-4}$.

3 Discussion and conclusion

The use of fiber delivery and a fiber beam-coupler for beam combination has significantly improved the robustness and wavelength tuning capability of the sensor. During routine operation, the DFG power level was found to be relatively stable for extended periods (for example 3.5% power decrease over 15 h). In addition the mechanical fiber coupling of the diode lasers did not need to be adjusted over several months of laboratory operation. To ensure stable sensor operation, care needed to be taken in packaging of the optical fibers, as any movement or pressure on the optical fibers affects the polarization of the pump beams and hence decreases the DFG conversion efficiency. Furthermore, the alignment was maintained (indicated by a constant DFG power level) when the sensor was relocated to an outside environment. These results are in contrast to our experience with the operation of DFG sensors based on discrete optics that required periodic minor re-alignments because of mirror and lens mount relaxation [3, 4]. In addition by utilizing an efficient high-power Yb-doped fiber amplifier we have eliminated the need for a high-power narrow-linewidth source. This requirement has been replaced by a low-power ($\sim$ several mW) diode or fiber laser seed source which can operate anywhere within the broad gain bandwidth of the Yb fiber amplifier (1020–1120 nm).

In Fig. 7 we have presented spectra of 6 common trace and pollutant species to demonstrate the versatility of this diode-laser-based DFG sensor. The specific spectral lines we have used for detection of each molecule were chosen on the basis of the expected concentrations present and known interfering species. However because of the extended continuous tuning range of this sensor, alternative absorption lines could be chosen for detection of low/high gas concentrations or in the presence of interfering molecular absorptions.

From this work, it was deduced that the current detection sensitivity is limited by the occurrence of etalons in the baseline, presently corresponding to absorbances of $\pm 2 \times 10^{-4}$. To compensate for these etalons and increase the absolute sensitivity of the absorption measurement, the use of a dual-beam spectroscopic configuration is expected to increase the routine detection limit to $\approx 5 \times 10^{-5}$. This will involve a wedged beam-sampling mirror placed prior to the multi-pass cell which directs a small amount of the beam to a second detector, thereby allowing the nonlinear baseline to be normalized using the sampled baseline. This technique will not remove the fringes that originate from the multiple mirror reflections in the multi-pass cell, but it is possible to use a digital notch filter to reduce these etalon fringes. For extended operation the frequency drift of the diode lasers must be controlled. This is particularly pronounced until the sensor suitcase reaches a steady-state temperature. Active temperature control of the DBR diode laser will require a frequency reference based on an appropriate spectral feature acquired from a reference gas cell (which can be periodically inserted into the beam path). Furthermore, a PPLN crystal with a 'fan-out' QPM grating design [15] will replace the discrete channel PPLN crystal which will permit continuous DFG wavelength scans to be conducted by synchronously tuning one of the pump wavelengths while translating the crystal. DFG power scaling using in-line fiber amplifiers [16] is expected to increase the available mid-IR DFG power by factors of 10 to 100, thereby improving the detector signal-to-noise, or allowing the use of IR detectors operating at room temperature without the need of Peltier cooling.

In conclusion, we have demonstrated a narrow-bandwidth DFG sensor with a 3.25–4.30 μm tuning range and generating up to 3 μW in the spectroscopically important 3–5 μm 'fingerprint' region. By fiber-coupling the pump sources and using a fiber coupler for combining the pump beams, routine alignment tasks have been eliminated. We have demonstrated sensitive, selective, and real-time detection of CH_4 at 3.3 μm by monitoring a calibrated mixture of CH_4 (1773 ppb) over a 20-min period and measuring a concentration of 1829.5 ppb with standard deviation of $\pm 0.8\%$. The measured standard deviation error corresponds to an absorption sensitivity of $\pm 2 \times 10^{-4}$. Furthermore, we have demonstrated the versatility of this sensor by recording spectra of six trace gas species: CO_2 (4.19 μm), N_2O (3.89 μm), H_2CO (3.53 μm), HCl (3.52 μm), NO_2 (3.47 μm), and CH_4 (3.30 μm). It will be possible to use the same device architecture in the future to extend the current spectral regime to longer wavelengths (5–16 μm) by using quasi-phasematched GaAs when this material becomes available [17, 18].

Acknowledgements. Financial support was provided by the National Aeronautics and Space Administration (NASA), the Texas Advanced Technologies Program, the National Science Foundation, and the Welch Foundation.

References

1. K.P. Petrov, L. Goldberg, W.K. Burns, R.F. Curl, F.K. Tittel: Opt. Lett. **21**, 86 (1996)
2. T. Töpfer, K.P. Petrov, Y. Mine, D. Jundt, R.F. Curl, F.K. Tittel: Appl. Opt. **36**, 8042 (1997)
3. D. Richter, D.G. Lancaster, R.F. Curl, W. Neu, F.K. Tittel: Appl. Phys. B **67**, 347 (1998)
4. D.G. Lancaster, D. Richter, R.F. Curl, F.K. Tittel: Appl. Phys. B **67**, 339 (1998)

5. K.P. Petrov, R.F. Curl, F.K. Tittel: Appl. Phys. B **66**, 531 (1998)
6. M. Seiter, D. Keller, M.W. Sigrist: Appl. Phys. B **67**, 351 (1998)
7. L. Goldberg, J. Koplow, D.G. Lancaster, R.F. Curl, F.K. Tittel: Opt. Lett. **23**, 1517 (1998)
8. D.G. Lancaster, L. Goldberg, J. Koplow, R.F. Curl, F.K. Tittel: Electron. Lett. **34**, 13, 1345 (1998)
9. J.P. Koplow, L. Goldberg, D.A.V. Kliner: IEEE Phot. Tech. Lett. **10**, 793 (1998)
10. L. Goldberg, B. Cole, E. Snitzer: Electron. Lett. **33**, 2127 (1997)
11. L. Lefort, K. Puech, S.D. Butterworth, Y.P. Svirko, G.W. Ross, D.C. Hanna, D.H. Jundt: CtuC1, CLEO 98
12. P. Canarelli, Z. Benko, R.F. Curl, F.K. Tittel: J. Opt. Soc. Am. B **9**, 197 (1992)
13. D.H. Jundt: Opt. Lett. **22**, 1553 (1997)
14. Courtesy of E. Dlugokencky, NOAA, Climate Monitoring & Diagnostic Laboratory, Boulder CO
15. P.E. Powers, T.J. Kulp, S.E. Bisson: Opt. Lett. **23**, 159 (1998)
16. L. Goldberg, J. Koplow, D.A.V. Kliner: Opt. Lett. **24**, 673 (1999)
17. D. Zheng, L.A. Gordon, Y.S. Wu, R.S. Feigelson, M.M. Fejer, R.L. Byer: Opt. Lett. **23**, 1010 (1998)
18. L.A. Eyres, C.B. Ebert, J.S. Harris Jr, M.M. Fejer: CNOM Annual Report 1997-1998, Stanford University